Available online at www.eccomasproceedia.org
Eccomas Proceedia UNCECOMP (2021) 354-370

ECCOMAS
Proceedia

UNCECOMP 2021
4th ECCOMAS Thematic Conference on
Uncertainty Quantification in Computational Sciences and Engineering
M. Papadrakakis, V. Papadopoulos, G. Stefanou (eds.)
Streamed from Athens, Greece, 28 -30 June 2021

ASSESSMENT OF VARIANTS OF THE METHOD OF MOMENTS AND POLYNOMIAL CHAOS APPROACHES TO AERODYNAMIC UNCERTAINTY QUANTIFICATION

E.M. Papoutsis-Kiachagias[1], V.G. Asouti[1] and K.C. Giannakoglou[1]

[1]National Technical University of Athens,
Parallel CFD & Optimization Unit, School of Mechanical Engineering
Zografou Campus, 9 Iroon Polytechniou Str
e-mail: {vpapout,vasouti,kgianna}@mail.ntua.gr

Abstract. *In real life problems uncertainties, for instance through uncertain boundary conditions or manufacturing imperfections, may affect the performance of an aerodynamic shape significantly. In order to measure the impact of uncertainties on the performance of an aerodynamic shape, statistical moments (usually the mean value and variance) of the Quantity of Interest (QoI, e.g. the lift or drag forces) have to be quantified through Uncertainty Quantification (UQ) techniques. This paper compares a number of variants of the Method of Moments (MoM) and the non-intrusive polynomial chaos (niPCE) approaches to UQ. Regarding the MoM, first- and second-order derivatives of the QoI with respect to the uncertain variables are necessary for formulating its first-(FOSM) and second-order (SOSM) variants, respectively. These are computed using a combination of continuous adjoint and direct differentiation of the governing (flow) equations. The statistical moments of the QoI can, then, easily be computed in terms of the QoI value and derivatives computed at the mean values of the uncertain variables. The results of the above-mentioned MoM variants are additionally compared to a number of niPCE variants developed and utilized by the authors in the past. The UQ variants of MoM and niPCE are then compared in terms of cost and accuracy of the computed statistical moments of the QoI. Comparisons also include results of the Monte Carlo method which acts as the reference method. The two benchmark cases used for the comparison include an airfoil under uncertain flow conditions and fluid properties as well as the DrivAer car model, under uncertain flow conditions.*

Keywords: Uncertainty Quantification, Method of Moments, Polynomial Chaos, Continuous Adjoint, Aerodynamics

ISSN:2623-3339
Peer-review under responsibility of the organizing committee of UNCECOMP 2021.
doi: 10.7712/120221.8043.19104

1 INTRODUCTION

A number of UQ approaches have been developed during the last years to help propagate the uncertainty from the inputs of the aerodynamic analysis problem (e.g. uncertain boundary conditions) to the QoI. A recent review of many of them and their incoorporation into robust design optimization loops with a focus on air vehicles can be found in [1]. In general, most UQ methods have a cost that scales with a power of the number M of the uncertain variables $c_i, i \in [1, M]$, making UQ computationally feasible for problems with only a moderate M. This paper focuses on some variants of the Method of Moments (MoM), [2, 3, 4, 5], and non-Intrusive Polynomial Chaos Expansion (niPCE) [6, 7, 8, 9] with a potential for a relatively low UQ cost and compares them in terms of cost and accuracy of computation of the statistical moments of the QoI; Monte Carlo (MC) acts as the reference method for computing the latter.

According to the MoM, the QoI (usually lift or drag for external aerodynamics problems) is expanded into a Taylor series in terms of $\boldsymbol{c}$. The statistical moments of the QoI are, then, obtained analytically by using this expansion in the integrals that define them. By keeping only the first-order term in the Taylor expansion and computing the first two statistical moments of the QoI, namely its mean and standard deviation, a First-Order Second-Moment (FOSM) UQ method is formulated [4]. If second-order terms are also maintained in the Taylor expansion, a Second-Order Second-Moment (SOSM) approach is devised. The FOSM approach calls for the computation of first-order derivatives of the QoI with respect to (w.r.t.) $\boldsymbol{c}$ while the SOSM approach additionally requires second-order derivatives, a.k.a. the Hessian matrix. First-order derivatives w.r.t. $\boldsymbol{c}$ are computed based on the continuous adjoint method developed by the group of authors in the past [10], at a cost that is independent of the value of M. As discussed in sections 2 and 4, this gives rise to the only UQ method known to the authors with a cost that does not scale with M. The most efficient method to compute second-order derivatives requires the combined use of adjoint and direct differentiation (DD, being the equivalent of the tangent-linear mode in an Automatic Differentiation tool), with a cost that scales linearly with M [11].

Additionally, a number of niPCE approaches are presented and compared to the two MoM variants. These include a) standard quadrature niPCE , b) regression-assisted niPCE computations based on at least as many QoI evaluations as the number of polynomial weights, [9, 12], and c) an adjoint-assisted regression approach by using the sensitivity derivatives of the QoI w.r.t. $\boldsymbol{c}$, to reduce the computational cost [13]. These variants were also compared to each other in terms of cost and accuracy by the authors in [14] and will not, thus, be analyzed in detail herein.

The rest of this paper is structured as follows: in section 2, the mathematical background of the MoM is presented, including the flow and adjoint equations, as well as the combination of adjoint and DD for the computation of the Hessian matrix. In section 3, the niPCE variants are presented in brief. In section 4, the cost of the two studied MoM variants is compared to that of the aforementioned niPCE approaches and, in section 5, the results of the developed MoM variants are compared with each other as well as with those obtained by niPCE and verified with reference results produced using MC simulations. Finally, conclusions are drawn in section 6.

2 MoM FRAMEWORK

2.1 Flow Equations and QoI

The cases examined in this paper are governed by the steady-state Navier-Stokes PDEs for incompressible flows,

$$R^p = -\frac{\partial v_j}{\partial x_j} = 0 \tag{1a}$$

$$R^v_i = v_j\frac{\partial v_i}{\partial x_j} - \frac{\partial \tau_{ij}}{\partial x_j} + \frac{\partial p}{\partial x_i} = 0, \quad i = 1,2,3, \tag{1b}$$

where v_i are the velocity components, $\tau_{ij} = (\nu+\nu_t)\left(\frac{\partial v_i}{\partial x_j} + \frac{\partial v_j}{\partial x_i}\right)$ the stress tensor components, p the (relative to the exit/reference) static pressure divided by the constant density, ν the (constant) kinematic viscosity of the fluid and ν_t the turbulent viscosity, computed only for turbulent flows. Twice repeated indices within the same term imply summation. In cases were turbulent flow are studied, the Spalart–Allmaras turbulence model [15] is used to effect closure; according to the latter, the turbulent viscosity is given by $\nu_t = \widetilde{\nu} f_{v_1}$ and computed after solving the PDE

$$R^{\widetilde{\nu}} = v_j\frac{\partial \widetilde{\nu}}{\partial x_j} - \frac{\partial}{\partial x_j}\left[\left(\nu+\frac{\widetilde{\nu}}{\sigma}\right)\frac{\partial \widetilde{\nu}}{\partial x_j}\right] - \frac{c_{b2}}{\sigma}\left(\frac{\partial \widetilde{\nu}}{\partial x_j}\right)^2 - \widetilde{\nu}P(\widetilde{\nu}) + \widetilde{\nu}D(\widetilde{\nu}) = 0, \tag{2}$$

for the turbulence variable $\widetilde{\nu}$. In the above equation, the production and destruction terms are given by $P(\widetilde{\nu}) = c_{b1}\widetilde{Y}$ and $D(\widetilde{\nu}) = c_{w1}f_w(\widetilde{Y})\frac{\widetilde{\nu}}{\Delta^2}$ respectively, with $\widetilde{Y} = f_{v_3}Y + \frac{\widetilde{\nu}}{\Delta^2\kappa^2}f_{v_2}$, $Y = \|\vec{S}\| = \|e_{ijk}\frac{\partial v_k}{\partial x_j}\|$ the vorticity magnitude and Δ the distance from the wall.

Dealing with external aerodynamics (flows around bodies such as airfoils or cars), eqs. 1 are associated with the following set of boundary conditions,

$$S_I\begin{cases} \boldsymbol{v} = |v_\infty|[cos(\alpha_\infty)\ sin(\alpha_\infty)]^T \\ \dfrac{\partial p}{\partial x_j}n_j = 0 \\ \widetilde{\nu} = ct \end{cases} \qquad S_W\begin{cases} v_i = 0 \\ \dfrac{\partial p}{\partial x_j}n_j = 0 \\ \widetilde{\nu} = 0 \end{cases} \qquad S_O\begin{cases} \dfrac{\partial v_i}{\partial x_j}n_j = 0 \\ p = 0 \\ \dfrac{\partial \widetilde{\nu}}{\partial x_j}n_j = 0, \end{cases} \tag{3}$$

where S_W is the contour of the aerodynamic body and S_I and S_O the parts of the farfield boundary in which the flow enters and exits the domain. Overall, $S = S_I \cup S_O \cup S_W$ is the boundary of the computational domain Ω and $|v_\infty|$, α_∞ are the farfield velocity magnitude and angle, respectively.

Without loss in generality, the drag or lift force coefficients,

$$J = \frac{\int_{S_W}(p\delta^j_i - \tau_{ij})n_j r_i}{N_F}dS, \quad N_F = \frac{1}{2}A_{ref}U^2_{ref}, \tag{4}$$

is the QoI throughout this paper, where $\boldsymbol{r}$ is the unit vector aligned with/perpendicular to the farfield velocity for the drag/lift computation, in the absence of uncertainties, A_{ref} is a reference area and U_{ref} is a reference velocity magnitude, usually coinciding with that of the farfield velocity.

2.2 MoM-based UQ

In the MoM, the QoI is developed using a Taylor expansion around the mean values of the uncertain variables, $\overline{\boldsymbol{c}}$; the order of the MoM is defined by the largest order of the derivatives of

the QoI w.r.t. $\boldsymbol{c}$ retained in the Taylor expansion,

$$J(\overline{\boldsymbol{c}}+\Delta\boldsymbol{c}) = J|_{\overline{\boldsymbol{c}}} + \left.\frac{\delta J}{\delta c_i}\right|_{\overline{\boldsymbol{c}}} \Delta c_i + \frac{1}{2}\left.\frac{\delta^2 J}{\delta c_i \delta c_j}\right|_{\overline{\boldsymbol{c}}} \Delta c_i \Delta c_j + O(\Delta \boldsymbol{c}^3). \tag{5}$$

The FOSM approach is formulated by retaining only $\delta J/\delta c_i$ in eq. 5, substituting it into the expressions of the mean value (μ_J) and standard deviation (σ_J) of the QoI and analytically integrating, to obtain, [4],

$$\mu_J(\boldsymbol{c}) = J|_{\overline{\boldsymbol{c}}}, \qquad \sigma_J(\boldsymbol{c}) = \sqrt{\sum_{i=1}^{M}\left[\frac{\delta J}{\delta c_i}\right]_{\overline{\boldsymbol{c}}}^2 \sigma_i^2}, \tag{6}$$

with σ_i standing for the known standard deviation of the i-th uncertain variable. In the FOSM approach, the expressions of μ_J and σ_J, eqs. 6, are independent of the probability density function (PDF) of $\boldsymbol{c}$. Hence, the FOSM-based UQ method can be used with any PDF. In order to avoid any misinterpretation regarding the summation convention, the summation symbol is retained whenever deemed necessary.

If, additionally, we assume that the uncertain variables follow a normal distribution and maintain the second-order derivatives in eq. 5, the SOSM-based statistical moments of J can be computed through

$$\mu_J(\boldsymbol{c}) = J|_{\overline{\boldsymbol{c}}} + \frac{1}{2}\sum_{i=1}^{M}\left[\frac{\delta^2 J}{\delta c_i^2}\right]_{\overline{\boldsymbol{c}}}\sigma_i^2, \qquad \sigma_J(\boldsymbol{c}) = \sqrt{\sum_{i=1}^{M}\left[\frac{\delta J}{\delta c_i}\right]_{\overline{\boldsymbol{c}}}^2\sigma_i^2 + \frac{1}{2}\sum_{i=1}^{M}\sum_{j=1}^{M}\left[\frac{\delta^2 J}{\delta c_i \delta c_j}\right]_{\overline{\boldsymbol{c}}}^2\sigma_i^2\sigma_j^2}, \tag{7}$$

requiring the additional computation of second-order derivatives w.r.t. $\boldsymbol{c}$. It is important to note that, in contrast to other UQ methods like niPCE and MC that rely on flow evaluations in a number of combinations of values of the uncertain variables, the MoM depends only on flow and derivative evaluations performed at the nominal operating conditions $\overline{\boldsymbol{c}}$; for the sake of convenience, the latter index will be omitted hereafter.

The computation of the first- and second-order derivatives required by the above-mentioned MoM is described in brief in the sections that follow.

2.3 Computation of $\frac{\delta J}{\delta c_l}$

First-order derivatives are computed using the continuous adjoint method. According to the latter, an augmented QoI is defined as

$$L = J + \int_\Omega u_i R_i^v d\Omega + \int_\Omega q R^p d\Omega + \int_\Omega \widetilde{\nu_a} R^{\widetilde{\nu}} d\Omega, \tag{8}$$

where Ω is the computational domain, u_i the adjoint velocity components, q the adjoint pressure and $\widetilde{\nu_a}$ the adjoint turbulence variable. Then, eq. 8 is differentiated w.r.t. $\boldsymbol{c}$. After setting the multipliers of $\delta v_i/\delta c_l$, $\delta p/\delta c_l$ and $\delta\widetilde{\nu}/\delta c_l$ to zero in the field integrals of the developed form of

$\delta J/\delta c_l$, the continuous adjoint PDEs for incompressible, turbulent flows are derived [10],

$$R^q = -\frac{\partial u_j}{\partial x_j} = 0 \tag{9a}$$

$$R^u_i = u_j\frac{\partial v_j}{\partial x_i} - \frac{\partial (v_j u_i)}{\partial x_j} - \frac{\partial \tau^a_{ij}}{\partial x_j} + \frac{\partial q}{\partial x_i} + \widetilde{\nu}_a\frac{\partial \widetilde{\nu}}{\partial x_i} - \frac{\partial}{\partial x_l}\left(\widetilde{\nu}_a\widetilde{\nu}\frac{\mathcal{C}_Y}{Y}e_{mjk}\frac{\partial v_k}{\partial x_j}e_{mli}\right) = 0\ ,\ i=1,2,3 \tag{9b}$$

$$R^{\widetilde{\nu_a}} = -\frac{\partial (v_j\widetilde{\nu}_a)}{\partial x_j} - \frac{\partial}{\partial x_j}\left[\left(\nu+\frac{\widetilde{\nu}}{\sigma}\right)\frac{\partial \widetilde{\nu}_a}{\partial x_j}\right] + \frac{1}{\sigma}\frac{\partial \widetilde{\nu}_a}{\partial x_j}\frac{\partial \widetilde{\nu}}{\partial x_j} + 2\frac{c_{b2}}{\sigma}\frac{\partial}{\partial x_j}\left(\widetilde{\nu}_a\frac{\partial \widetilde{\nu}}{\partial x_j}\right) + \widetilde{\nu}_a\widetilde{\nu}\mathcal{C}_{\widetilde{\nu}}$$
$$+\frac{\partial \nu_t}{\partial \widetilde{\nu}}\frac{\partial u_i}{\partial x_j}\left(\frac{\partial v_i}{\partial x_j}+\frac{\partial v_j}{\partial x_i}\right) + (-P+D)\,\widetilde{\nu}_a = 0, \tag{9c}$$

where $\tau^a_{ij} = (\nu+\nu_t)\left(\frac{\partial u_i}{\partial x_j}+\frac{\partial u_j}{\partial x_i}\right)$ are the adjoint stress tensor components. The $\mathcal{C}_{\tilde{\nu}}$ and $\mathcal{C}_Y$ expressions can be found in [16].

After satisfying the continuous adjoint PDEs and differentiating eq. 4 w.r.t. $\boldsymbol{c}$, the remaining terms of $\delta J/\delta c_l = \delta L/\delta c_l$ read [17],

$$\frac{\delta J}{\delta c_l} = \int_{S_W}\left(\frac{\delta p}{\delta c_l}\delta^j_i - \frac{\delta \tau_{ij}}{\delta c_l}\right) r_i n_j dS + \int_S \left(u_i v_j n_j + \tau^a_{ij}n_j - qn_i + \widetilde{\nu}_a\widetilde{\nu}\frac{\mathcal{C}_Y}{Y}e_{mjk}\frac{\partial v_k}{\partial x_j}e_{moi}n_o\right)\frac{\delta v_i}{\delta c_l}dS$$
$$+\int_S u_i n_i \frac{\delta p}{\delta c_l}dS - \int_S u_i n_j \frac{\delta \tau_{ij}}{\delta c_l}dS, - \int_\Omega u_i \frac{\partial}{\partial x_j}\left(\frac{\partial v_i}{\partial x_j}+\frac{\partial v_j}{\partial x_i}\right)\frac{\delta \nu}{\delta c_l}d\Omega. \tag{10}$$

It should be noted that $\boldsymbol{r}$ and U_{ref} in eq. 4 are not considered to change w.r.t. $\boldsymbol{c}$. Following the methodology presented in [10], the adjoint boundary conditions are formulated by eliminating boundary integrals containing variations of v_i, p, τ_{ij} and $\widetilde{\nu}$, where necessary, and read

$$S_I\begin{cases} u_i = 0 \\ \dfrac{\partial q}{\partial x_j}n_j = 0 \\ \widetilde{\nu}_a = 0 \end{cases}, S_W\begin{cases} u_i = -\dfrac{r_i}{N_F} \\ \dfrac{\partial q}{\partial x_j}n_j = 0 \\ \widetilde{\nu}_a = 0 \end{cases}, S_O\begin{cases} q = u_n v_n + 2\nu\dfrac{\partial u_i}{\partial x_j}n_i n_j \\ +\widetilde{\nu}_a\widetilde{\nu}\dfrac{\mathcal{C}_Y}{Y}e_{mjk}\dfrac{\partial v_k}{\partial x_j}e_{moi}n_o n_i, \\ u_t v_n + \nu\left(\dfrac{\partial u_i}{\partial x_j}+\dfrac{\partial u_j}{\partial x_i}\right)n_j t_i \\ +\widetilde{\nu}_a\widetilde{\nu}\dfrac{\mathcal{C}_Y}{Y}e_{mjk}\dfrac{\partial v_k}{\partial x_j}e_{moi}n_o t_i = 0 \\ v_j n_j\widetilde{\nu}_a + \left(\nu+\dfrac{\widetilde{\nu}}{\sigma}\right)\dfrac{\partial \widetilde{\nu}_a}{\partial x_j}n_j = 0, \end{cases} \tag{11}$$

where $\boldsymbol{n}$ and $\boldsymbol{t}$ are the normal and tangential unit vectors and indices n and t indicate the normal and tangential velocity components, respectively. A realistic assumption is that the solution of the adjoint equations costs approximately as much as that of the flow equations. Hence, the flow and adjoint fields are computed at the cost of one Equivalent Flow Solution (EFS) each. EFS is used as the cost unit for the UQ methods that are compared in this paper.

Herein, uncertainties are associated with the flow conditions and properties. In specific, the uncertain variables are the free-stream flow angle, $c_1 = \alpha_\infty$, the magnitude of the farfield velocity, $c_2 = |v_\infty|$ and the flow kinematic viscosity, $c_3 = \nu$. Though the MoM has a comparative cost advantage to other UQ methods as M gets higher, even a case of $M = 3$ is enough for

demonstrating the benefits of the method. Considering the adjoint boundary conditions, the gradient of J w.r.t. c_l is computed as follows,

$$\frac{\delta J}{\delta c_l} = \int_{S_I} \left(\tau_{ij}^a n_j - q n_i\right) \frac{\delta v_i}{\delta c_l} dS - \int_\Omega u_i \frac{\partial}{\partial x_j}\left(\frac{\partial v_i}{\partial x_j} + \frac{\partial v_j}{\partial x_i}\right) \frac{\delta \nu}{\delta c_l} d\Omega. \tag{12}$$

Since $v_i|_{S_I}$ directly depends on $\boldsymbol{c}$, eq. 3, $\frac{\delta v_i}{\delta c_l}\Big|_{S_I}$ is computed analytically as,

$$\frac{\delta \boldsymbol{v}}{\delta c_1}\Big|_{S_I} = |v_\infty| \begin{bmatrix} -sin(\alpha_\infty) \\ cos(\alpha_\infty) \end{bmatrix} \quad \frac{\delta \boldsymbol{v}}{\delta c_2}\Big|_{S_I} = \begin{bmatrix} cos(\alpha_\infty) \\ sin(\alpha_\infty) \end{bmatrix} \quad \frac{\delta \boldsymbol{v}}{\delta c_3}\Big|_{S_I} = \begin{bmatrix} 0 \\ 0 \end{bmatrix} \tag{13}$$

and $\frac{\delta \nu}{\delta c_l}$ is straightforward. Hence, all components of $\delta J/\delta c_l$ are computed at a cost of 2 EFS, irrespective of M. This makes the FOSM an affordable UQ method for problems with many uncertain variables.

2.4 Computation of $\frac{\delta^2 J}{\delta c_l \delta c_m}$

The SOSM approach additionally requires the computation of $\frac{\delta^2 J}{\delta c_l \delta c_m}$, a.k.a. the Hessian of J w.r.t. $\boldsymbol{c}$. The Hessian matrix can be computed using all possible combinations of adjoint and DD as outlined in [11], there for compressible flows. Based on [11], the most cost-efficient approach to compute the Hessian matrix is based on the DD of the flow equations to compute $\frac{\delta v_i}{\delta c_m}$, $\frac{\delta p}{\delta c_m}$ and the adjoint method to avoid the computation of $\frac{\delta^2 v_i}{\delta c_m \delta c_l}$, $\frac{\delta^2 p}{\delta c_m \delta c_l}$; the latter approach is also mentioned as the DD-AV approach in [11] and has a cost of $M + 2$ EFS for computing the Hessian matrix; this includes the solution of the flow and adjoint PDEs. In what follows, the same approach is presented in brief for laminar, incompressible flows.

Let the derivative of any flow quantity ϕ w.r.t. the uncertain variables c_l be denoted as

$$\widetilde{\phi}^l = \frac{\delta \phi}{\delta c_l} \tag{14}$$

Then, the derivative of the QoI w.r.t. $\boldsymbol{c}$ is written as

$$\frac{\delta J}{\delta c_l}\Big|_{DD} = -\int_{S_W} \delta_l^3 E_{ij} \frac{n_j r_i}{N_F} dS - \int_{S_W} \nu \widetilde{E_{ij}}^l \frac{n_j r_i}{N_F} dS + \int_{S_W} \widetilde{p}^l \frac{n_i r_i}{N_F} dS \tag{15}$$

where $E_{ij} = \frac{\partial v_i}{\partial x_j} + \frac{\partial v_j}{\partial x_i}$ is the strain tensor and δ_l^3 is the Kronecker symbol. In order to compute $\widetilde{E_{ij}}^l$ and $\widetilde{p}^l$, the flow equations, eq. 1, are directly differentiated w.r.t. $\boldsymbol{c}$, yielding $l \in [1, 3]$ (in general $l \in [1, M]$) sets of PDEs

$$\widetilde{R^p}^l = -\frac{\partial \widetilde{v_j}^l}{\partial x_j} = 0 \tag{16a}$$

$$\widetilde{R_i^v}^l = \widetilde{v_j}^l \frac{\partial v_i}{\partial x_j} + v_j \frac{\partial \widetilde{v_i}^l}{\partial x_j} - \nu \frac{\partial \widetilde{E_{ij}}^l}{\partial x_j} - \delta_l^3 \frac{\partial E_{ij}}{\partial x_j} + \frac{\partial \widetilde{p}^l}{\partial x_i} = 0, \quad i = 1, 2, 3 \tag{16b}$$

from which $\widetilde{p}^l$ and $\widetilde{v_i}^l$ (and, in consequence, $\widetilde{E_{ij}}^l$) can be computed. Eqs. 16 are accompanied by their boundary conditions, which are derived by differentiating eq. 3 w.r.t. $\boldsymbol{c}$, yielding

$$S_I \begin{cases} \widetilde{\boldsymbol{v}}^l = \dfrac{\delta \boldsymbol{v}}{\delta c_l} (eq.\ 13) \\ \dfrac{\partial \widetilde{p}^l}{\partial x_j} n_j = 0 \end{cases} , S_W \begin{cases} \widetilde{v_i}^l = 0 \\ \dfrac{\partial \widetilde{p}^l}{\partial x_j} n_j = 0 \end{cases} , S_O \begin{cases} \dfrac{\partial \widetilde{v_i}^l}{\partial x_j} n_j = 0 \\ \widetilde{p}^l = 0. \end{cases} \tag{17}$$

The Hessian is computed by differentiating eq. 15 once more w.r.t. $\boldsymbol{c}$ and augmenting the outcome with the field integrals of the second-order derivatives of the flow equations, multiplied with appropriate adjoint fields, i.e.

$$\frac{\delta^2 J}{\delta c_m \delta c_l} = \frac{\delta}{\delta c_m} \left(\left. \frac{\delta J}{\delta c_l} \right|_{DD} \right) + \int_\Omega u_i \frac{\delta^2 R_i^v}{\delta c_m \delta c_l} d\Omega + \int_\Omega q \frac{\delta^2 R^p}{\delta c_m \delta c_l} d\Omega \tag{18}$$

As it will be proven, the adjoint fields on the right hand side (r.h.s.) of eq. 18 coincide with those computed through eq. 9 (excluding terms stemming from the differentiation of the turbulence model). To help simplify the mathematical notation, let

$$\overline{\phi}^{l,m} = \frac{\delta^2 \phi}{\delta c_m \delta c_l} \tag{19}$$

denote the second-order derivative of any flow quantity ϕ w.r.t. the uncertain variables. Differentiating eq. 15 w.r.t. c_l yields

$$\begin{aligned} \frac{\delta}{\delta c_m} \left(\left. \frac{\delta J}{\delta c_l} \right|_{DD} \right) = &- \int_{S_W} \delta_l^3 \widetilde{E_{ij}}^m \frac{n_j r_i}{N_F} dS - \int_{S_W} \delta_m^3 \widetilde{E_{ij}}^l \frac{n_j r_i}{N_F} dS - \int_{S_W} \nu \overline{E_{ij}}^{l,m} \frac{n_j r_i}{N_F} dS \\ &+ \int_{S_W} \overline{p}^{l,m} \frac{n_i r_i}{N_F} dS \end{aligned} \tag{20}$$

Assuming that eqs. 16 have already been solved, the first two integrals on the r.h.s. of eq. 20 can readily be computed. However, evaluating the last two integrals of the r.h.s. of the same equation would require the computation of $\overline{E_{ij}}^{l,m}$ and $\overline{p}^{l,m}$ that would come at a cost scaling with M^2. To avoid this exponential rise of the UQ cost w.r.t. M, an adjoint system of equations can be formulated expanding the second and third terms on the r.h.s. of eq. 18 as

$$\begin{aligned} &\int_\Omega u_i \frac{\delta^2 R_i^v}{\delta c_m \delta c_l} d\Omega + \int_\Omega q \frac{\delta^2 R^p}{\delta c_m \delta c_l} d\Omega = \\ &\quad \int_\Omega \left[u_j \frac{\partial v_j}{\partial x_i} - \frac{\partial (v_j u_i)}{\partial x_j} - \frac{\partial \tau_{ij}^a}{\partial x_j} + \frac{\partial q}{\partial x_i} \right] \overline{v_i}^{l,m} d\Omega - \int_\Omega \frac{\partial u_i}{\partial x_i} \overline{p}^{l,m} d\Omega \\ &\quad + \int_S \left(u_i v_j n_j + \tau_{ij}^a n_j - q n_i \right) \overline{v_i}^{l,m} dS - \int_S \nu u_i n_j \overline{E_{ij}}^{l,m} dS + \int_S u_i n_i \overline{p}^{l,m} dS \\ &\quad + \int_\Omega u_i \widetilde{v_j}^l \frac{\partial \widetilde{v_i}^m}{\partial x_j} d\Omega + \int_\Omega u_i \widetilde{v_j}^m \frac{\partial \widetilde{v_i}^l}{\partial x_j} d\Omega - \int_\Omega u_i \delta_l^3 \frac{\partial \widetilde{E_{ij}}^m}{\partial x_j} d\Omega - \int_\Omega u_i \delta_m^3 \frac{\partial \widetilde{E_{ij}}^l}{\partial x_j} d\Omega \end{aligned} \tag{21}$$

By setting the multipliers of $\overline{v_i}^{l,m}$ and $\overline{p}^{l,m}$ in the field integrals of eq. 21 to zero, the latter becomes independent of second-order derivatives of the flow variables w.r.t. $\boldsymbol{c}$ in the interior of the computational domain. This process leads to the formulation of an adjoint system of PDEs that is identical to the one presented in eq. 9. The corresponding adjoint boundary conditions

coincide with those of eq. 11. The remaining terms of eq. 20 and 21 give raise to the expression of the Hessian matrix

$$\frac{\delta^2 J}{\delta c_m \delta c_l} = -\int_{S_W} \delta_l^3 \widetilde{E_{ij}}^m \frac{n_j r_i}{N_F} dS - \int_{S_W} \delta_m^3 \widetilde{E_{ij}}^l \frac{n_j r_i}{N_F} dS + \int_{S_I} \left(\tau_{ij}^a n_j - q n_i\right) \overline{v_i}^{l,m} dS + \int_\Omega u_i \widetilde{v_j}^l \frac{\partial \widetilde{v_i}^m}{\partial x_j} d\Omega + \int_\Omega u_i \widetilde{v_j}^m \frac{\partial \widetilde{v_i}^l}{\partial x_j} d\Omega - \int_\Omega u_i \delta_l^3 \frac{\partial \widetilde{E_{ij}}^m}{\partial x_j} d\Omega - \int_\Omega u_i \delta_m^3 \frac{\partial \widetilde{E_{ij}}^l}{\partial x_j} d\Omega \tag{22}$$

where the components of $\overline{v_i}^{l,m}$ at the inlet are given by

$$\overline{\boldsymbol{v}}^{1,1} = -\boldsymbol{v}, \quad \overline{\boldsymbol{v}}^{1,2} = \overline{\boldsymbol{v}}^{2,1} = \begin{bmatrix} -sin(\alpha_\infty) \\ cos(\alpha_\infty) \end{bmatrix}, \quad \overline{\boldsymbol{v}}^{2,2} = \overline{\boldsymbol{v}}^{1,3} = \overline{\boldsymbol{v}}^{3,1} = \overline{\boldsymbol{v}}^{2,3} = \overline{\boldsymbol{v}}^{3,2} = \boldsymbol{0} \tag{23}$$

2.5 Flowchart of the MoM approach to UQ

The process of computing μ_J and σ_J using the MoM is summarized in the flowchart that follows, including the computational cost of each step.

1 Solution of the flow equations (eqs. 1) at $\boldsymbol{c}=\overline{\boldsymbol{c}}$, at the cost of 1 EFS, to obtain the v_i, p and $\widetilde{\nu}$ fields, followed by the computation of J at $\overline{\boldsymbol{c}}$.
2 Solution of the adjoint equations (eqs. 9), at the cost of 1 EFS, to obtain the u_i, q and $\widetilde{\nu_a}$ fields.
3 Computation of $\frac{\delta J}{\delta c_m}, m \in [1, M]$ from eq. 12 (negligible cost).
4 **if** *MoM == FOSM* **then**
5 Computation of μ_J and σ_J through eq. 6 (negligible cost).
6 **else if** *MoM == SOSM* **then**
7 Solution of the DD equations, eqs. 16, at the cost of M EFS, to obtain the $\widetilde{v_i}^l$ and $\widetilde{p}^l$ fields, for $l \in [1, M]$.
8 Computation of $\frac{\delta^2 J}{\delta c_m \delta c_l}$ from eq. 22 with $m, l \in [1, M]$ (negligible cost).
9 Computation of μ_J and σ_J through eq. 7 (negligible cost).

3 niPCE-BASED UQ

Assuming that J depends on the vector of uncertain variables $c_i, i \in [1, M]$, niPCE approximates J as

$$J(\boldsymbol{c}) \approx \sum_{i=0}^{Q-1} J_i H_i(\boldsymbol{c}), \tag{24}$$

where $Q = \frac{(M+k)!}{M!k!}$, k is the largest degree of the multivariate orthogonal polynomials $H_i(\boldsymbol{c})$ and J_i are their corresponding weights.

The multivariate polynomials $H_i(\boldsymbol{c})$ are constructed through the products of univariate orthogonal polynomials that depend on the statistical distribution of the uncertain variables and are chosen from the Wiener-Askey family, [8]. For all applications presented in this paper,

all uncertain variables are assumed to follow a Gaussian distribution and p are the normalized probabilists' Hermite polynomials.

Assuming that the polynomial weights J_i are known, the first and second statistical moments of the QoI are given by, [8]

$$\mu_J = J_0,\ \sigma_J = \sqrt{\sum_{i=1}^{Q-1} J_i^2} \tag{25}$$

What remains to compute μ_J and σ_J and perform UQ is to compute the coefficients J_i. These are defined through the Galerkin projection of J to $H_i(\boldsymbol{c})$, i.e.

$$J_i = \int \cdots \int J(\boldsymbol{c}) H_i(\boldsymbol{c}) W(\boldsymbol{c}) d\boldsymbol{c} \tag{26}$$

where $W(\boldsymbol{c})$ is the product of the PDFs $w_i, i \in [1, M]$ of the uncertain variables. Numerical approaches for computing J_i, with emphasis on cost reduction in cases of $M \gg$ are described in sections 3.1 and 3.2.

3.1 Gauss Quadrature

Since the polynomial coefficients are given by multidimensional integrals, eq. 26, they can be approximated numerically, by evaluating J at appropriate values of $\boldsymbol{c}$. Taking advantage of the fact that the integrand of eq. 26 is a weighted polynomial, Gauss Quadrature rules, [18], can be used to numerically compute J_i. The type of Gauss Quadrature depends on the form of $H_i(\boldsymbol{c})$ which, in turn, depends on the assumed statistical distribution of $\boldsymbol{c}$. For the Gaussian distribution assumed herein, Gauss–Hermite Quadrature (GHQ) is used.

Computing J_i requires $(k+1)^M$ evaluations of J. This exponential dependency of the cost on M leads to the so-called "curse of dimensionality", making the GQ-based niPCE variant quite costly for cases with even a modest number of uncertain variables. To compensate for its relatively high computational cost, the GQ-based niPCE approach is quite accurate when compared to MC, as it will be shown in section 5.

3.2 Regression-based niPCE and Acceleration through Adjoint-based Gradients

An alternative for computing J_i can be pursued by means of a regression which avoids numerically integrating eq. 26 to compute J_i instead, it approximates them using a more stochastic approach, [9, 12]. In specific, if J is evaluated at L different $\boldsymbol{c}$ values, eq. 24 can be used to formulate the following system of equations

$$\begin{bmatrix} H_0(\boldsymbol{c}_1) & \dots & H_{Q-1}(\boldsymbol{c}_1) \\ \vdots & \ddots & \vdots \\ H_0(\boldsymbol{c}_L) & \dots & H_{Q-1}(\boldsymbol{c}_L) \end{bmatrix} \begin{bmatrix} J_0 \\ \vdots \\ J_{Q-1} \end{bmatrix} = \begin{bmatrix} J(\boldsymbol{c}_1) \\ \vdots \\ J(\boldsymbol{c}_L) \end{bmatrix} \tag{27}$$

with L equations and Q unknowns. If $L = Q = \frac{(M+k)!}{M!k!}$, then eq. 27 can be solved directly to compute the Q unknown coefficients at a cost of Q EFS. To increase accuracy, J is usually oversampled and eq. 27 corresponds to a least squares problem, [19]. For what follows, an oversampling by a factor of $r = 2$ is used, i.e. $L = 2Q$. What remains to be decided are the L different $\boldsymbol{c}$ points in which J should be evaluated to obtain the right-hand-side (r.h.s.) of eq. 27.

This is still an open issue in the corresponding literature and a number of approaches have been proposed, like random sampling, Latin Hypercube sampling and Hammersley sequence sampling, [20]. In the applications presented in this report, a Latin Hypercube Sampling (LHS) is used. The cost of the regression-based niPCE is compared to the other UQ variants presented in this paper in Table 1.

One flow solution (J evaluation) contributes one line in the system of eq. 27. Adding more lines to eq. 27 for each flow solution which is carried out could further accelerate the UQ process. To do so, the (continuous) adjoint method for computing sensitivity derivatives presented in section 2.3 can be employed. The latter can provide all the components of $\delta J/\delta c_i, i \in [1, M]$ by additionally solving the adjoint PDEs, at a cost of 1 EFS. Assuming an oversampling by a factor of $r > 1$, the sampling points required to obtain rQ equations for computing J_i are[1] $P = \left\lfloor \frac{r(M+k)!}{(M+1)!k!} \right\rfloor = \lfloor \frac{rQ}{M+1} \rfloor$, i.e. approximately one order of M lower than that of the typical regression approach given by eq. 27. The adjoint-assisted regression approach reads, [13]

$$\begin{bmatrix} H_0(\boldsymbol{c}_1) & \dots & H_{Q-1}(\boldsymbol{c}_1) \\ \frac{\partial H_0}{\partial c_1}(\boldsymbol{c}_1) & \dots & \frac{\partial H_{Q-1}}{\partial c_1}(\boldsymbol{c}_1) \\ \vdots & \vdots & \vdots \\ \frac{\partial H_0}{\partial c_M}(\boldsymbol{c}_1) & \dots & \frac{\partial H_{Q-1}}{\partial c_M}(\boldsymbol{c}_1) \\ \vdots & \ddots & \vdots \\ H_0(\boldsymbol{c}_L) & \dots & H_{Q-1}(\boldsymbol{c}_L) \\ \frac{\partial H_0}{\partial c_1}(\boldsymbol{c}_L) & \dots & \frac{\partial H_{Q-1}}{\partial c_1}(\boldsymbol{c}_L) \\ \vdots & \vdots & \vdots \\ \frac{\partial H_0}{\partial c_M}(\boldsymbol{c}_L) & \dots & \frac{\partial H_{Q-1}}{\partial c_M}(\boldsymbol{c}_L) \end{bmatrix} \begin{bmatrix} J_0 \\ \vdots \\ J_{Q-1} \end{bmatrix} = \begin{bmatrix} J(\boldsymbol{c}_1) \\ \frac{\delta J}{\delta c_1}(\boldsymbol{c}_1) \\ \vdots \\ \frac{\delta J}{\delta c_M}(\boldsymbol{c}_1) \\ \vdots \\ J(\boldsymbol{c}_L) \\ \frac{\delta J}{\delta c_1}(\boldsymbol{c}_L) \\ \vdots \\ \frac{\delta J}{\delta c_M}(\boldsymbol{c}_L) \end{bmatrix} \tag{28}$$

and its cost, taking into consideration that each of the P sampling points costs one flow and one adjoint solution, is given in Table 1. It can be observed that adjoint-assisted regression has the lowest cost of all niPCE variants for $M > 1$, with the gain increasing considerably in the presence of many uncertain variables. Indicatively, for the widely used case of $M = 3, k = 2$, adjoint-assisted regression has half the cost of the typical regression and almost one third of the GQ one.

It should be noted that the cost of the adjoint-assisted regression mentioned in Table 1 is valid in cases with only one QoI. Since the computation of sensitivity derivatives for many QoI requires the solution of as many adjoint PDEs, the cost benefit of the adjoint-assisted regression is mitigated in such cases. For the general case with N_Q QoI and an oversampling by a factor of r, the cost of the adjoint-assisted regression approach is $(N_Q + 1)\left\lfloor \frac{r(M+k)!}{(M+1)!k!} \right\rfloor$ EFS. Neglecting the potential necessity for rounding, the cost ratio of the adjoint-assisted regression and the typical regression is $\frac{N_Q+1}{M+1}$. This means that in cases with more uncertain variables than QoI, adjoint-assisted regression is still more efficient than the typical regression. On the other hand, in cases where $N_Q > M$, the typical regression should be preferred.

[1] It should be noted that $\frac{r(M+k)!}{(M+1)!k!}$ may not be an integer, so it has to be rounded to the closest one. The $\lfloor . \rfloor$ sign indicates the floor operation.

4 COST COMPARISON OF THE VARIOUS UQ METHODS

For a problem with M uncertain variables, the cost of the two MoM variants analyzed in section 2.2 is compared with that of the PCE variants briefly presented in section 3. Assuming an niPCE UQ approach with a degree of k, the cost of the niPCE and MoM variants studied thus far is summarized in Table 1. Since one set of adjoint PDEs has to be solved to compute the gradient of each QoI, the UQ variants that employ it have a cost that depends on the number of QoI, N_Q. For the regression-based niPCE variants, r is the oversampling factor.

Method	Cost (EFS)	Sample points
FOSM	$1 + N_Q$	1
SOSM	$M + 1 + N_Q$	1
niPCE - GQ	$(k+1)^M$	$(k+1)^M$
niPCE - Regression	$\frac{r(M+k)!}{M!k!}$	$\frac{r(M+k)!}{M!k!}$
niPCE - Regression - Adjoint	$(N_Q+1)\left\lfloor \frac{r(M+k)!}{(M+1)!k!} \right\rfloor$	$\left\lfloor \frac{r(M+k)!}{(M+1)!k!} \right\rfloor$

Table 1: CPU cost, measured in EFS, for computing (μ_J, σ_J) with a number of niPCE and MoM variants.

Since SOSM treats treats J as a second-order polynomial of $\boldsymbol{c}$, it is interesting to compare its cost with the niPCE variants in case $k = 2$, i.e. when niPCE also treats J as a second-order polynomial. This is summarized in Table 2, for various M values. It can be observed that for $M > 1$, SOSM has half the cost of the cheapest niPCE variant and a significantly smaller one than all other niPCE variants as M increases.

niPCE - GQ / niPCE - Regression / niPCE - Regression -Adjoint / SOSM						
k \ M	1	2	3	4	5	6
2	**3**/6/6/**3**	9/12/8/**4**	27/20/10/**5**	81/30/12/**6**	243/42/14/**7**	729/56/16/**8**

Table 2: CPU cost, measured in EFS, for computing (μ_J, σ_J) with a number of niPCE variants and the SOSM approach, for a single QoI. All approaches included in this table approximate J as a second-order polynomial of $\boldsymbol{c}$. An oversampling by a factor of 2 is used for both regression-based approaches. The result with the lowest cost is marked in bold for each (M, k) pair.

5 VERIFICATION – APPLICATIONS

The results of the MoM variants presented in section 2 are compared with each other, with various niPCE variants presented in section 3 and, for the 2D case, verified using MC simulations. Upon obtaining these J values, μ_J and σ_J can directly be computed through their definitions. Due to its simplicity, MC is used as a benchmark method for validating other UQ methods. On the other hand, the fact that it requires a very large number of J evaluations makes it computationally infeasible for the $3D$ case examined in Section 5.2.

5.1 NACA0012 airfoil

In the first case examined, UQ is performed for the flow over the NACA0012 isolated airfoil, fig. 1, under uncertain flow conditions and properties. The flow is laminar, $Re = 2000$, drag and lift coefficients are used as the QoI and uncertainties emanate from the farfield velocity and angle, as well as the fluid kinematic viscosity. The denominator of the force coefficients is considered constant. The mean values and standard deviations of the three uncertain variables $(M = 3)$ following a normal distribution are listed in Table 3. The flow is solved on grid consisting of 37800 quadrilateral elements.

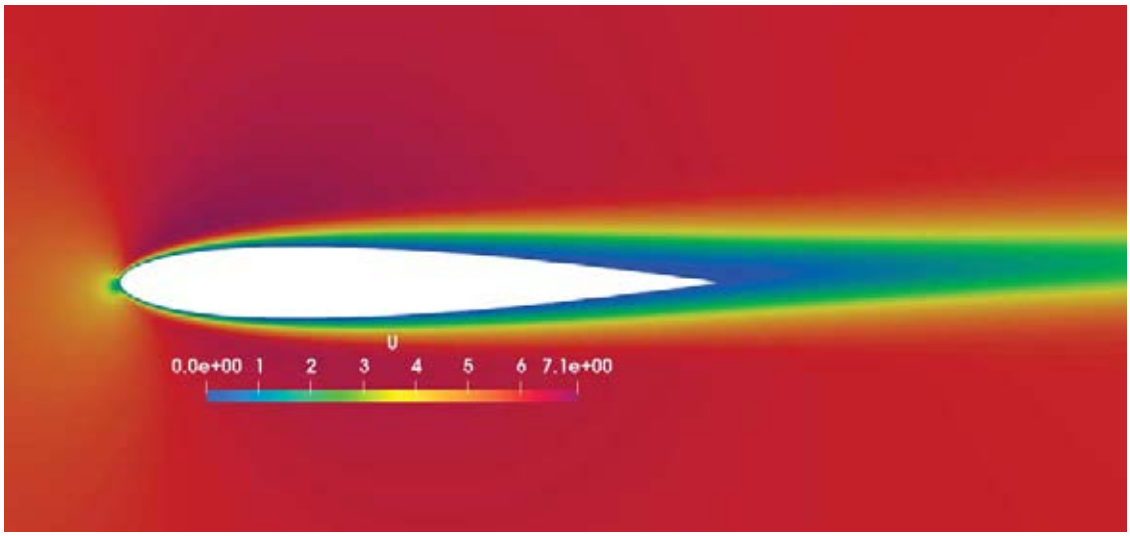

Figure 1: NACA0012: velocity magnitude contours around the airfoil, computed using the mean values of the uncertain variables.

Uncertain variable	μ	σ
Farfield velocity magnitude (m/s)	6	0.6
Farfield velocity angle (deg)	2	0.2
Kinematic viscosity (m^2/s)	3×10^{-3}	1×10^{-4}

Table 3: NACA0012: Mean values and standard deviations of the uncertain variables.

Using the mean values and standard deviations of Table 3, two UQ scenarios are studied. In the first one, only the farfield velocity magnitude and angle are considered as uncertain variables $(M = 2)$ while in the second one, all three uncertain variables are used. In both scenarios, second-order polynomials are used $(k = 2)$ for the niPCE variants and MC relies upon 1000 evaluations. The μ_J and σ_J approximations based on the MoM variants presented in section 2 along with the corresponding values computed based on a number of niPCE variants presented in section 3 are listed in Tables 4 and 5 for $M = 2$ and $M = 3$, respectively, together with their relative error compared to MC.

Compared to MC, FOSM computes μ_J with a relative error that is smaller than 0.38% and SOSM has an even smaller maximum deviation from MC of 0.19%. For the drag coefficient, SOSM even has the smaller deviation from MC than all other UQ methods tested herein. On the other hand, deviations of the MoM-based σ_J values from MC are higher that the ones of the niPCE variants, especially for the lift coefficient, for which a deviation of 8.8% is observed. From the FOSM- and SOSM-based statistical moments in Tables 4 and 5, it can be

observed that SOSM consistently improves the μ_J predictions over FOSM, this is not however the case for σ_J. This can be explained by analyzing the FOSM- and SOSM-based expressions of σ_J, eqs. 6 and 7, respectively. From there, it can be observed that the SOSM-based σ_J value will always be larger than the FOSM-based one, due to the addition of a positive quantity $\left(\frac{1}{2}\sum_{i=1}^{M}\sum_{j=1}^{M}\left[\frac{\delta^2 J}{\delta c_i \delta c_j}\right]_{\overline{c}}^2 \sigma_i^2 \sigma_j^2\right)$ to the FOSM-based σ_J^2 value. Hence, if the FOSM-based σ_J value is overestimated, SOSM can only increase this deviation from the reference value of MC. The MoM-based σ_J values for the drag coefficient are more accurate than those for the lift coefficient (max. deviation of 1.2% from MC).

Summarizing the findings of this study, we can deduce that both FOSM and SOSM are quite accurate when approximating the μ_J values, with the SOSM consistently outperforming the FOSM method for this statistical moment. On the other hand, the MoM-based σ_J values may deviate from the reference ones. Nevertheless, the small cost of the MoM-based approach and especially that of FOSM that is independent of M, makes it a useful tool for robust design optimization loops, as presented for instance in [21].

Method	Cost	Lift		Drag	
		μ_J (% Diff)	σ_J (% Diff)	μ_J (% Diff)	σ_J (% Diff)
FOSM	**2**	0.09538 (-0.38)	0.02070 (8.8)	0.08463 (-0.2)	0.01257 (0.9)
SOSM	4	0.09557 (-0.19)	0.02070 (8.8)	**0.08472 (-0.16)**	0.01257 (0.9)
niPCE-GQ	9	**0.09577 (0.02)**	0.01912 (0.5)	0.08463 (-0.2)	0.01254 (0.6)
niPCE-Regression	12	0.09571 (-0.04)	**0.01911 (0.4)**	0.08619 (1.6)	0.01204 (-3)
niPCE-Regression-Adjoint	8	0.09583 (0.08)	0.02012 (5)	0.08463 (-0.2)	**0.01253 (0.5)**
MC	1000	0.09575	0.01902	0.08486	0.01246

Table 4: NACA0012: Case with $M=2$. Mean value and standard deviation of the drag and lift coefficients as the QoI computed with the MoM variants of section 2 and the niPCE variants of section 3, compared with the outcome of MC. Numbers in the parentheses indicative the relative error w.r.t. MC. Cells corresponding to the lowest cost and smallest absolute value of relative error are marked in bold.

Method	Cost	Lift		Drag	
		μ_J (% Diff)	σ_J (% Diff)	μ_J (% Diff)	σ_J (% Diff)
FOSM	**2**	0.09538 (-0.36)	0.02071 (8.77)	0.08463 (-0.24)	0.01265 (1.2)
SOSM	5	0.09557 (-0.17)	0.02071 (8.77)	**0.84723 (-0.13)**	0.01265 (1.2)
niPCE-GQ	27	**0.09575 (0.02)**	**0.01913 (0.5)**	0.08462 (-0.25)	0.01263 (0.99)
niPCE-Regression	20	0.09584 (0.11)	0.01915 (0.61)	0.08463 (-0.23)	**0.01261 (0.85)**
niPCE-Regression-Adjoint	10	0.09529 (-0.47)	0.02001 (5.08)	0.08462 (-0.25)	0.01262 (0.9)
MC	1000	0.09573	0.01904	0.08483	0.01251

Table 5: NACA0012: Case with $M=3$. Notation as in Table 4.

5.2 DrivArer Car Model

The DrivArer car model, [22], developed by the Institute of Aerodynamics and Fluid Mechanics of TU Munich, is studied in this section. In specific, the fast-back configuration with a smooth underbody, with mirrors and wheels (F_S_wm_ww) is used as a test case, fig. 2. The drag coefficient is used as the QoI and the fafield velocity magnitude and angle are treated as uncertain variables, with mean values and standard deviations given by Table 6. The denominator of the drag coefficient is considered constant. For the niPCE variants, a max. polynomial degree of $k=2$ is selected.

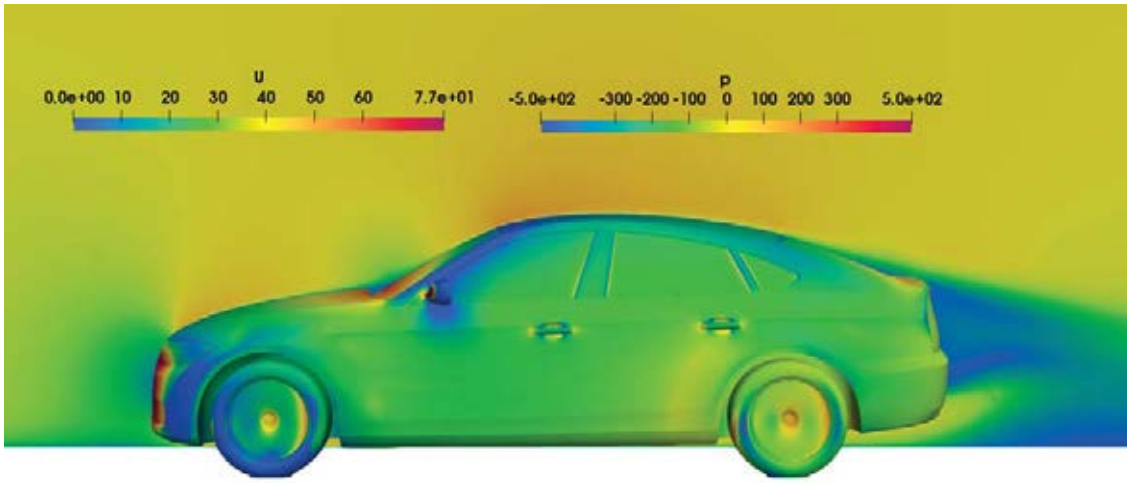

Figure 2: DrivAer: pressure contours on the car surface and velocity contours plotted on a slice along the symmetry plane of the car, computed using the mean values of the uncertain variables.

Uncertain variable	μ	σ
Farfield velocity magnitude (m/s)	38.9	1
Farfield velocity angle (deg)	0	2

Table 6: DrivAer: Mean values and standard deviations of the uncertain variables.

A hex-dominated mesh of 12 million cells is used and the steady-state RANS equations are solved, together with the Spalart–Allmaras turbulence model, [15]. Each flow evaluation takes approximately an hour in 120 cores. Due to the large computational cost, MC is not performed for this test case. The FOSM approach is instead compared to the GQ and regression variants of niPCE. The latter is conducted using the $(k{+}1)^M = 9$ Gauss nodes used in GQ as the samples of the regression method. It can be seen that the μ_J computed by the FOSM method does not differ much from the niPCE results (relative difference of 1.9%). Regarding σ_J, a more significant deviation of 12% is observed.

Method	Cost	Drag	
		μ_J	σ_J
FOSM	2	0.32663	0.01668
niPCE-GQ	9	0.33305	0.01908
niPCE-Regression	9	0.33306	0.01946

Table 7: DrivAer: Mean value and standard deviation of the drag coefficient computed with FOSM and two niPCE variants.

6 SUMMARY – CONCLUSIONS

In this paper, two Method of Moments approaches, namely First- and Second-Order Second-Moment (FOSM and SOSM), used for propagating uncertainties from the Quantities of Interest, were analysed in terms of cost and predictive accuracy.

The FOSM approach requires the sensitivity derivatives of the QoI w.r.t. the uncertain variables, which were computed herein using continuous adjoint, at a cost of one Equivalent Flow

Solution, irrespective of the number of uncertain variables M. This gives rise to a UQ method with a cost that does not scale with M and is equal to 2 EFS, making it ideal for UQ problems with many uncertain variables. SOSM additionally requires the computation of the Hessian matrix of the QoI with respect to the uncertain variables. This is computed using a combination of the adjoint fields already computed for FOSM and the Direct Differentiation of the flow equations, computing the variations of the flow fields w.r.t. the uncertain variables at a cost that scales linearly with M; the total cost of the SOSM-based UQ process is $M + 2$ EFS. Even though the cost of SOSM scales with M, the fact that it only scales linearly and with a unitary multiplier of M makes it twice as efficient as the cheapest non-intrusive Polynomial Chaos Expansion method, which also utilized adjoint-based sensitivity derivatives of the QoI w.r.t. the uncertain variables. Nevertheless, the need for second-order derivatives makes its development and utilization tedious for applications with complex numerical models, like turbulent flows involving wall functions.

Regarding the accuracy of the two MoM approaches, the first two statistical moments of the lift and drag coefficients were computed for two UQ problems pertaining to the flow around a 2D airfoil, with uncertainties emanating from the farfield conditions and the fluid kinematic viscosity; these statistical moments were then verified with results obtained from Monte Carlo simulations, acting as the reference method, as well as values obtained through a number of niPCE variants. It was observed that both FOSM and SOSM compute the mean value of the QoI with high accuracy, with SOSM consistently outperforming FOSM. On the other hand, both MoM approaches exhibited a considerable difference (8.8%) from the MC results for the standard deviation of the lift coefficient, with a better behaviour observed for σ_J of the drag coefficient. In addition, it was noticed that if FOSM over-predicts the standard deviation, SOSM can only make the prediction worse since it adds an always constant contribution to the σ_J computed by FOSM.

Finally, the FOSM-based statistical moments of the drag coefficient of the DrivAer car model were compared to those computed with niPCE; the farifield velocity magnitude and angle were considered as the uncertain variables. The mean value was computed with an acceptable accuracy (1.9% deviation from the niPCE results), however the standard deviation exhibited a higher relative difference of 12%. Nevertheless, the low cost of the FOSM approach makes it an ideal candidate as the UQ method used to compute the objective functions of robust design optimization loops, as already presented by the group of authors in other publications.

Acknowledgments

This project has received funding from the Hellenic Foundation for Research and Innovation (HFRI) and the General Secretariat for Research and Technology (GSRT), under grant agreement No 603.

REFERENCES

[1] Z. Huan, G. Zhenghong, X. Fang, and Z. Yidian. Review of robust aerodynamic design optimization for air vehicles. *Archives of Computational Methods in Engineering*, 26:685–732, 2019.

[2] R.W. Waters and L. Huyse. Uncertainty analysis for fluid mechanics with applications. *NASA/CR 2002*, 211449, 2002.

[3] M.M. Putko, P.A. Newman, A.C. Taylor, and L.L. Green. Approach for uncertainty propagation and robust design in CFD using sensitivity derivatives. In *AIAA Paper 2001-2528, 15th Computational Fluid Dynamics Conference*, Anaheim, CA, 2001.

[4] E.M. Papoutsis-Kiachagias, D.I. Papadimitriou, and K.C. Giannakoglou. Robust design in aerodynamics using third-order sensitivity analysis based on discrete adjoint. Application to quasi-1D flows. *International Journal for Numerical Methods in Fluids*, 69(3):691–709, 2012.

[5] D.I. Papadimitriou and K.C. Giannakoglou. Third-order sensitivity analysis for robust aerodynamic design using continuous adjoint. *International Journal for Numerical Methods in Fluids*, 71(5):652–670, 2013.

[6] C. Lacor, C. Dinescu, C. Hirsch, and S. Smirnov. *Implementation of intrusive polynomial chaos in CFD codes and application to 3D Navier-Stokes*, pages 193–223. Springer International Publishing, 2013.

[7] C. Dinescu, S. Smirnov, C. Hirsch, and C. Lacor. Assessment of intrusive and non-intrusive non-deterministic CFD methodologies based on polynomial chaos expansion. *International Journal of Engineering Systems Modeling and Simulations*, 2:87–98, 2010.

[8] D. Xiu and G.M. Karniadakis. Modeling uncertainty in flow simulations via generalized polynomial chaos. *Journal of Computational Physics*, 187:137–167, 2003.

[9] D. Xiu and J. Hesthaven. High-order collocation methods for differential equations with random inputs. *SIAM Journal of Scientific Computing*, 27:1118–1139, 2005.

[10] E.M. Papoutsis-Kiachagias and K.C. Giannakoglou. Continuous adjoint methods for turbulent flows, applied to shape and topology optimization: Industrial applications. *Archives of Computational Methods in Engineering*, 23(2):255–299, 2016.

[11] D.I. Papadimitriou and K.C. Giannakoglou. Direct, adjoint and mixed approaches for the computation of Hessian in airfoil design problems. *International Journal for Numerical Methods in Fluids*, 56(10):1929–1943, 2008.

[12] D. Xiu. Fast numerical methods for stochastic computations: A review. *Communications in computational physics*, 5:242–222, 2009.

[13] J. Peng, J. Hampton, and A. Doostan. On polynomial chaos expansion via gradient-enhanced $l1$-minimization. *Journal of Computational Physics*, 310:440 – 458, 2016.

[14] E.M. Papoutsis-Kiachagias, V.G. Asouti, and K.C. Giannakoglou. Polynomial chaos-based, adjoint-enabled uncertainty quantification and robust design for aerodynamic problems. In *4th International Conference on Uncertainty Quantification in Computational Sciences and Engineering, UNCECOMP 2019*, Crete island, Greece, 24-26 June 2019.

[15] P. Spalart and S. Allmaras. A one-equation turbulence model for aerodynamic flows. In *AIAA Paper 1992-0439, 30th Aerospace Sciences Meeting and Exhibit*, Reno, Nevada, 6-9 January 1992.

[16] A.S. Zymaris, D.I. Papadimitriou, K.C. Giannakoglou, and C. Othmer. Continuous adjoint approach to the Spalart-Allmaras turbulence model for incompressible flows. *Computers & Fluids*, 38(8):1528–1538, 2009.

[17] I.S. Kavvadias, E.M. Papoutsis-Kiachagias, and K.C. Giannakoglou. On the proper treatment of grid sensitivities in continuous adjoint methods for shape optimization. *Journal of Computational Physics*, 301:1–18, 2015.

[18] GH. Golub and Welsch JH. Calculation of gauss quadrature rules. *Mathematics of Computation*, 22:221–230, 1969.

[19] H. Zhao, Z. Gao, Y. Gao, and C. Wang. Effective robust design of high lift NLF airfoil under multi-parameter uncertainty. *Aerospace Science and Technology*, 68:530–542, 2017.

[20] S. Hosder, R. Walters, and M. Balch. Efficient sampling for non-intrusive Polynomial Chaos applications with multiple uncertain input variables. In *48th AIAA/ASME/ASCE/AHS/ASC Structures, Structural Dynamics, and Materials Conference*, 2007.

[21] K.B. Fragkos, E.M. Papoutsis-Kiachagias, and K.C. Giannakoglou. pFOSM: An efficient algorithm for aerodynamic robust design based on continuous adjoint and matrix-vector products. *Computers & Fluids*, 181:57–66, 2019.

[22] A. Heft, T. Indinger, and N. Adams. Experimental and numerical investigation of the DrivAer model. In *ASME 2012, Symposium on Issues and Perspectives in Automotive Flows*, pages 41–51, Puerto Rico, USA, 8-12 July 2012.